High Power Laser Science and Engineering, (2024), Vol. 12, e62, 7 pages.
doi:10.1017/hpl.2024.45

HIGH POWER LASER SCIENCE AND ENGINEERING

RESEARCH ARTICLE

A simple and effective method for identifying the real sources of pre-pulses in CPA and OPCPA laser systems

Haidong Chen[1,2,†], Xun Chen[1,2,†], Xingyan Liu[1], Jiabing Hu[1], Peile Bai[1,2], Jiayan Gui[1], Xiaojun Yang[1], Kegui Xia[1], Fenxiang Wu[1], Zongxin Zhang[1], Yanqi Liu[1], Xinliang Wang[1], Yi Xu[1], and Yuxin Leng[1]

[1] *State Key Laboratory of High Field Laser Physics and CAS Center for Excellence in Ultra-intense Laser Science, Shanghai Institute of Optics and Fine Mechanics, Chinese Academy of Sciences, Shanghai, China*

[2] *Center of Materials Science and Optoelectronics Engineering, University of Chinese Academy of Sciences, Beijing, China*

(Received 19 April 2024; revised 12 June 2024; accepted 21 June 2024)

Abstract

The delay-shift of the pre-pulse may mislead the determination of its origination and cause problems for the temporal contrast improvement of high-peak-power lasers, especially when the corresponding post-pulse is beyond the time window of the measurement device. In this work, an empirical formula is proposed to predict the delay-shift of pre-pulses for the first time. The empirical formula shows that the delay-shift is proportional to the square of the post-pulse's initial delay, and also the ratio of the third-order dispersion to the group delay dispersion's square, which intuitively reveals the main cause for the delay-shift and may provide a convenient routing for identifying the real sources of pre-pulses in both chirped-pulse amplification (CPA) and optical parametric chirped-pulse amplification (OPCPA) systems. The empirical formula agrees well with the experimental results both in the CPA and the OPCPA systems. Besides, a numerical simulation is also carried out to further verify the empirical formula.

Keywords: chirped-pulse amplification; optical parametric chirped-pulse amplification; pre-pulse

1. Introduction

Thanks to the invention of the chirped-pulse amplification (CPA) technique, laser peak power has increased rapidly in the past decades from the gigawatt (GW) to the terawatt (TW) and petawatt (PW) level. It has become the main technical route to develop ultra-intense lasers worldwide[1–3]. Different from the radiation transition process in CPA systems, the optical parametric chirped-pulse amplification (OPCPA) is based on the nonlinear and instantaneous process, which directly transfers the pump energy to the signal. It is a promising technique to achieve high peak power due to the absence of the parasitic lasing effect. In addition, the nonlinear crystal deuterated potassium dihydrogen phosphate (DKDP) for OPCPA systems can provide a large aperture size of approximately 400 mm and large amplification bandwidth of more than 200 nm centered at 925 nm, which is beneficial to produce lasers with peak power up to several tens of PW[4–6]. Besides, combined with the CPA and OPCPA, hybrid laser systems have also been constructed[7,8]. In these ultra-intense laser systems, the parameter of temporal contrast (defined as the ratio of the peak intensity of the main pulse to the noise intensity) is crucially important. As the laser peak power increases, it should also be improved because noise with certain intensity would pre-ionize the target, which is detrimental to the interaction of the target and the main pulse[9,10].

The laser noise can be divided into three main categories. The first is amplified spontaneous emission or parametric fluorescence, which generally appears as ground noise extending to nanoseconds. It is usually improved by employing a high-energy and high-contrast seed based on the double CPA method[11–14] or reasonably designing the amplification gain[15–17]. The second is coherent noise, which exhibits an exponential rising edge with the temporal extent to several tens of picoseconds. In recent years, study on the origination of coherent noise[18–21] has been mainly focused

Correspondence to: X. Wang, Y. Xu, and Y. Leng, State Key Laboratory of High Field Laser Physics and CAS Center for Excellence in Ultra-intense Laser Science, Shanghai Institute of Optics and Fine Mechanics, Chinese Academy of Sciences, Shanghai 201800, China. Emails: wxl@siom.ac.cn (X. Wang); xuyi@siom.ac.cn (Y. Xu); lengyuxin@mail.siom.ac.cn (Y. Leng)

[†]These authors contributed equally to this work.

on spatiotemporal coupling. It can be significantly improved by changing the stretcher structure[22] or replacing it with a higher-surface-quality grating[23] and convex mirror[24] in the stretcher. The third is the pre-pulse on the nanosecond scale (ns pre-pulse) and the pre-pulse on the picosecond scale (ps pre-pulse). The ns pre-pulse is usually generated from regenerative amplifiers and multi-pass amplifiers. It can be improved by using pulse pickers[25] and optimizing the amplifier configuration[26].

The ps pre-pulse is generated firstly by the interference of the main pulse and post-pulse, and then the self-phase modulation[27,28] in CPA systems or the nonlinear gain and the coupled interaction between the signal pulse and pump pulse in OPCPA systems[29,30]. The post-pulse is usually created by the multiple surface reflections in the optical component. According to the early theoretical analysis, the ps pre-pulse would be produced at the symmetrical temporal position of the corresponding post-pulse. However, it was interesting that the pre-pulse was found to be delayed with respect to the symmetrical position in a real CPA system[28,31]. The delay-shift of the pre-pulse (defined as the time delay of the pre-pulse with respect to the symmetrical temporal position of the corresponding post-pulse) brings difficulties to identify the source of the pre-pulse, especially when the corresponding post-pulse is beyond the time window of the contrast measurement device (approximately 150 ps after the main pulse). Until recently, numerical results have indicated that the delay-shift originates from the high-order dispersion of the stretcher in CPA systems[32]. In addition, high-order dispersion is also the main cause of the delay-shift in OPCPA systems, which has been investigated numerically and experimentally[33]. However, analytical analysis has not been carried out yet. In order to better understand the generation of the pre-pulse, an analytical solution or empirical formula needs to be established.

In this work, we propose a simple empirical formula including the group delay dispersion (GDD), the third-order dispersion (TOD) and the initial delay of the post-pulse to estimate the delay-shift of pre-pulses. Based on the empirical formula, the actual temporal position of the pre-pulse or the post-pulse could be obtained. This empirical formula is compared to the experimental results in a broadband CPA system centered at 800 nm as well as in a broadband OPCPA system centered at 925 nm. Regardless of the type of pulse amplifier or pulse stretcher, the experimental results agree well with the empirical formula. A numerical simulation was also carried out to further verify the empirical formula.

2. Empirical formula

One key factor in the process of pre-pulse generation is that the pulse is nonlinearly modulated by the B-integral in CPA systems or the nonlinear gain in OPCPA systems. The common point in CPA and OPCPA systems is that this nonlinear modulation is directly connected to the initial temporal modulation caused by the interference of the main pulse and post-pulse. When the high-order dispersion of the stretcher is considered, the stretched temporal profile and the modulation frequency of the initial temporal modulation would be a little bit different compared to that in which only the GDD is considered, and delay-shift of the generated pre-pulse would also occur. Unfortunately, in this case the Fourier transformation between the temporal domain and the frequency domain of the modulated pulse is too complicated to be solved analytically. In other words, the analytical interpretation of the delay-shift affected by the high-order dispersion is difficult to obtain. However, according to the above analysis, we guess that the mechanism of the delay-shift could be very similar for the CPA and OPCPA, which is attributed to the complicated initial temporal modulation affected by the high-order dispersion. In addition, a previous numerical study indicated that TOD was more important for the origin of the delay-shift compared to other high-order dispersions[32]. In this paper, a simple empirical formula is proposed to estimate the delay-shift including GVD and TOD as below:

$$t_{\mathrm{delay}} = -k\frac{\phi^{(3)}}{\left(\phi^{(2)}\right)^2}t_{\mathrm{post}}^2, \tag{1}$$

where t_{delay} is the delay-shift of the pre-pulse; $\phi^{(2)}$ and $\phi^{(3)}$ are the GDD and TOD values of the stretcher, respectively; t_{post} is the initial delay of the post-pulse; and k is the empirical factor, which is set to 0.85. The positive value of t_{delay} denotes that the pre-pulse moves towards the main pulse, while the negative value of t_{delay} denotes that the pre-pulse moves away from the main pulse. In most ultra-intense laser systems, the TOD value is negative. As a result, t_{delay} calculated by Equation (1) is positive.

In the above formula, the delay-shift is proportional to the ratio of TOD to GDD's square. We can deduce that TOD could lead to the delay-shift of the pre-pulse. The delay-shift would be larger as the TOD increases, and a relatively large GDD value would suppress the increasement of the delay-shift. Besides, the delay-shift is proportional to the square of t_{post}. So, the delay-shift would be small when the post-pulse is near the main pulse, and the delay-shift would be obviously observed when the post-pulse is far from the main pulse. If t_{post} is known, the actual position of the pre-pulse can be calculated according to Equation (1) as below:

$$t_{\mathrm{pre}} = -t_{\mathrm{post}} + t_{\mathrm{delay}} = -t_{\mathrm{post}} - k\frac{\phi^{(3)}}{(\phi^{(2)})^2}t_{\mathrm{post}}^2. \tag{2}$$

Sometimes, the post-pulse is too far from the main pulse to be measured because the time window of the frequently used measurement device is limited to approximately 150 ps after the main pulse, and only the pre-pulse could be measured. If the delay-shift is also unknown, the post-pulse position would be difficult to locate accurately. However, thanks to

https://doi.org/10.1017/hpl.2024.45 Published online by Cambridge University Press

Equation (2), the post-pulse position can be calculated by the following:

$$t_{\text{post}} = \frac{-\left(\phi^{(2)}\right)^2 + \sqrt{\left(\phi^{(2)}\right)^4 - 4k\left(\phi^{(2)}\right)^2 \phi^{(3)} t_{\text{pre}}}}{2k\phi^{(3)}}. \quad (3)$$

With the knowledge of t_{post}, it would be easy to determine the thickness of the optical component that introduces the post-pulse, as below:

$$d = \frac{c}{2n} t_{\text{post}}, \quad (4)$$

where n is the refractive index of the optical component, d is the thickness of the transmission medium and c is the velocity of light.

It is also worth mentioning that the above formulae are independent of the stretcher type as well as the amplifier type. In the next section, we verify the accuracy of Equation (1) in real CPA and OPCPA systems. Once Equation (1) was verified, Equations (2)–(4) could be reliable for identifying the pre-pulse, post-pulse and the corresponding optical component that introduces the post-pulse.

3. Experimental results

3.1. Experiment on a CPA system

The experiment was carried out on the homemade 200 TW/24 fs/1 Hz Ti:sapphire laser[34,35]. It consisted of a Ti:sapphire oscillator, a single-grating Offner stretcher, a regenerative amplifier, a multi-pass amplifier, a power amplifier, a final amplifier and a vacuum compressor. The values of GDD, TOD, fourth-order dispersion (FOD) and fifth-order dispersion (FiOD) of the stretcher were 4.79×10^6 fs^2, -9.74×10^6 fs^3, 3.16×10^7 fs^4 and -1.42×10^8 fs^5, respectively. With the spectrum ranging from 750 to 850 nm, the pulse was temporally stretched to nearly 1.4 ns (full width). In this experiment, the power amplifier and the final amplifier were not in operation. The output energy of the multi-pass amplifier was approximately 40 mJ, corresponding to the B-integral value of approximately 0.037 rad.

Plane-parallel plates made of uncoated BK7 with different thicknesses of 1, 5, 10 and 15 mm were inserted separately before the multi-pass amplifier. Due to the double reflections of the transmitted pulse in the plates, the post-pulses at approximately 11, 51, 103 and 154.5 ps after the main pulse were produced. After the amplification and compression, the pre-pulses would be generated because of the B-integral. The temporal profile with a high dynamic range was measured by a commercial third-order cross-correlator (Amplitude, Sequoia).

The plate with thickness of 1 mm was firstly inserted in the system. The pre-pulse and the post-pulse were generated at approximately –11 and 11 ps, respectively. There is no obvious delay-shift because the post-pulse and pre-pulse were very close to the main pulse. According to Equation (1), the delay-shift calculated by the empirical formula was as small as 50 fs. When the 1 mm plate was replaced by the 5 mm plate, the real pre-pulse was generated at approximately –51 ps corresponding to the post-pulse at 52 ps, as depicted in Figure 1(a). As a result, the delay-shift appeared, and it was at 1 ps. The pre-pulse at –52 ps was a ghost pulse, which was caused by the mixing of the second harmonics of the post-pulse and the fundamental of the main pulse in the measurement device. Figure 1(b) illustrates the temporal profile when the 10 mm plate was inserted. The real pre-pulse was generated at approximately −99 ps, and the post-pulse was produced at approximately 103 ps. Thus, the corresponding delay-shift increased to 4 ps. The pre-pulse at –103 ps should be the ghost pulse. It could be observed that as the initial delay of the post-pulse increased, the delay-shift became larger. When the 15 mm plate was inserted, the real pre-pulse was generated at approximately –145.5 ps and the post-pulse was produced at 154.5 ps, as depicted in Figure 1(c). Thus, the corresponding delay-shift increased to 9 ps. The delay-shift calculated by the empirical formula was 8.5 ps, which was 0.5 ps lower than the experimental value. The pre-pulse at –154.5 ps should be the ghost pulse. The pre-pulse at approximately –109 ps existed even when the plate was not inserted, which might be generated by the Ti:sapphire crystal in the laser chain.

Figure 1(d) illustrates the delay-shift versus the initial delay of post-pulses, which was obtained by the empirical formula (blue line) and the experiment (black diamond). The formula agreed well with the experimental results, and the experimental values of delay-shift almost increased with the square of the initial delay of the post-pulse. The minor deviation between the formula and the experimental results could be explained by two reasons. On one hand, high-order dispersions such as FOD and FiOD, which were neglected in the empirical formula, may also contribute to the delay-shift. On the other hand, the pre-pulse was temporally distorted, and the duration of the pre-pulse was larger than that of the main pulse[33]. However, the empirical formula was unable to predict the temporal profile of the pre-pulse, which could also introduce the error of the formula.

3.2. Experiment on an OPCPA system

In order to verify the universality of the empirical formula, a similar experiment was carried out on the OPCPA front-end of the SEL-100 PW facility[6]. This OPCPA system provided an ultra-broadband seed ranging from 820 to 1030 nm. Different from the single-grating Offner stretcher in the above CPA system, a dedicated designed double-grating Offner stretcher was used in this facility for a better spatio-temporal quality[36]. The values of GDD, TOD, FOD and FiOD of this stretcher were 6.08×10^6 fs^2, -1.67×10^7 fs^3,

https://doi.org/10.1017/hpl.2024.45 Published online by Cambridge University Press

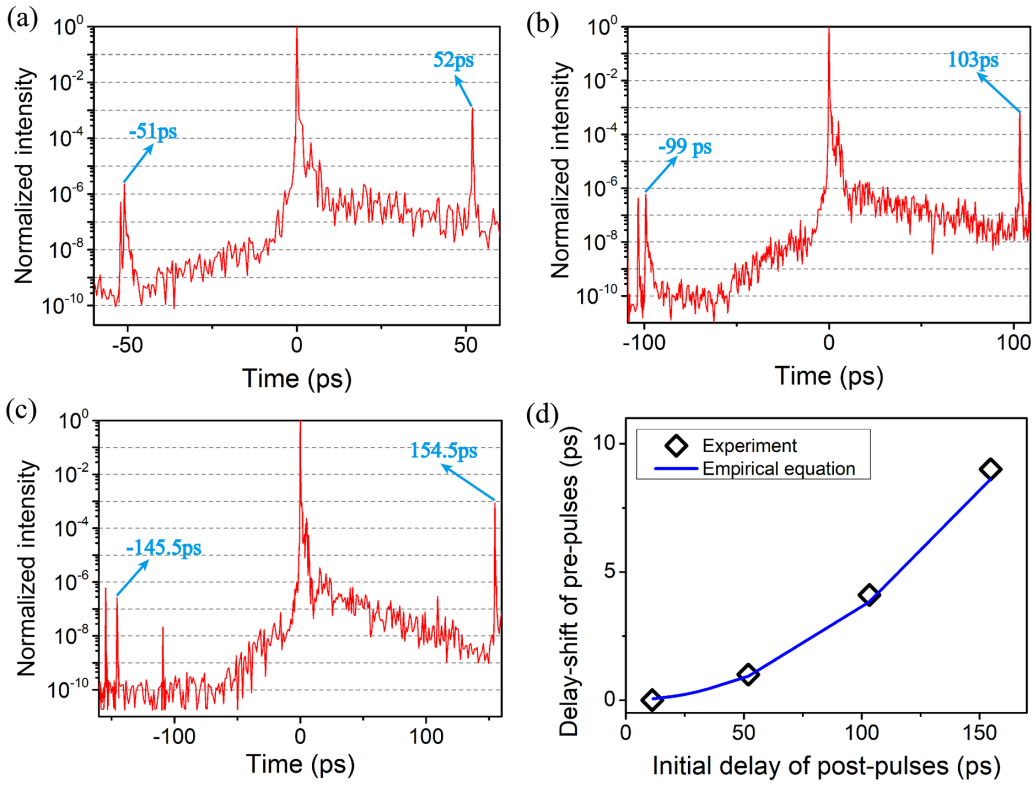

Figure 1. (a)–(c) The temporal profile when plane-parallel plates with thicknesses of 5, 10 and 15 mm were inserted into the CPA system. (d) The delay-shift versus the initial delay of post-pulses.

7.54×10^7 fs^4 and -4.72×10^8 fs^5, respectively. The stretched pulse duration was 3 ns (full width). Then the seed pulse passed through the three-stage optical parametric amplifier. In this experiment, the third amplifier stage was not in operation. The output energy of the two-stage amplifier was 488 mJ, and the repetition rate was 1 Hz. After the compressor, the pulse duration was compressed to about 15 fs.

The plane-parallel plates used in the above CPA system were also inserted before the second stage of the optical parametric amplifier. The delay-shift was also not observed when the 1 mm plate was inserted. Figures 2(a)–2(c) depict the output temporal profile when the plates with thicknesses of 5, 10 and 15 mm were inserted, respectively. The real pre-pulses were produced at approximately −51, −99 and −145 ps, respectively. The corresponding delay-shifts in the experiment were 1, 4 and 9.5 ps. According to the empirical formula, the calculated delay-shifts were 1, 4 and 9 ps, respectively, which were similar to the experimental values. As depicted in Figure 2(d), the measured delay-shift was still almost proportional to the square of the initial delay of the post-pulse. In addition to the pre-pulses generated by the post-pulse due to the double reflection in the plate, the pre-pulses due to the quartic reflection[33] were also measured. The delay-shift of these pre-pulses also agreed well with the empirical formula, but they are not discussed in detail in this paper for simplicity.

Consequently, the empirical formula was believed to be reliable in the above two ultra-intense systems. If there exists a new pre-pulse in these systems, Equations (3) and (4) could also be useful to locate the post-pulse and the optical component.

4. Further discussion on the delay-shift affected by $\phi^{(3)}/(\phi^{(2)})^2$

In the above section, the empirical formula was verified by two kinds of amplifiers based on different stretchers. However, coincidently, the values of $\phi^{(3)}/(\phi^{(2)})^2$ were 0.42 and 0.45 ns^{-1} in the CPA system and the OPCPA system, respectively, which were very similar. In the real system, the dispersion of the stretcher was dedicatedly designed, and could not be modified casually. In order to further investigate the delay-shift variation affected by $\phi^{(3)}/(\phi^{(2)})^2$, a simulation was carried out in this section based on the numerical method, which studied the pre-pulse in the CPA system[32]. GDD, TOD, FOD and FiOD were all taken into account in the simulation. The initial delay of the post-pulse in the simulation was 154.5 ps. The seed bandwidth, seed energy density and pump parameters in the simulation were similar to those in Section 3.1. The difference was that the values of $\phi^{(2)}$ and $\phi^{(3)}$ were both divided by the factor n ($n > 0$). Thus, the value of $\phi^{(3)}/(\phi^{(2)})^2$ was multiplied by the factor n.

https://doi.org/10.1017/hpl.2024.45 Published online by Cambridge University Press

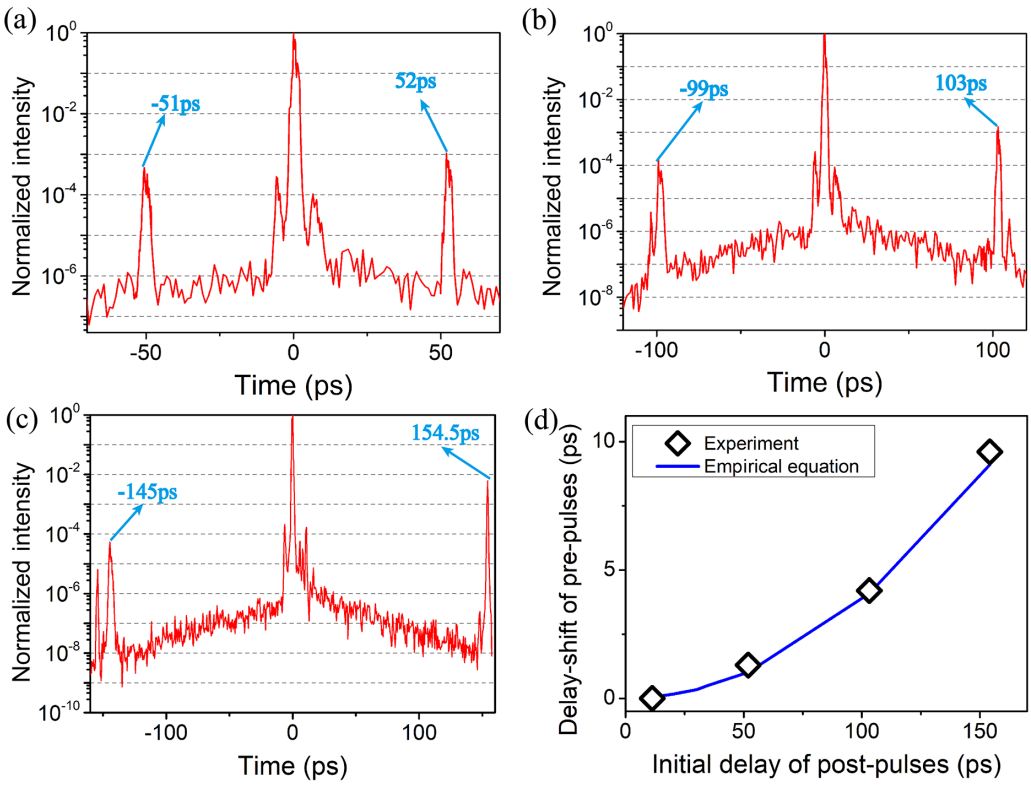

Figure 2. (a)–(c) The temporal profile when plane-parallel plates with thicknesses of 5, 10 and 15 mm were inserted into the OPCPA system. (d) The delay-shift versus the initial delay of post-pulses.

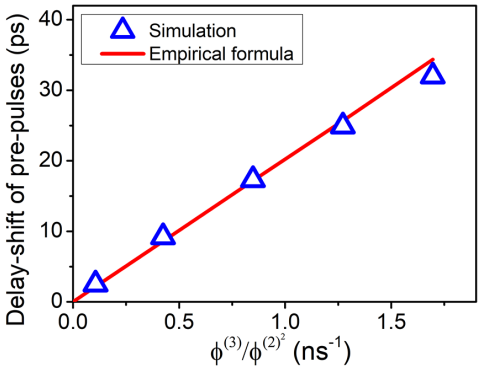

Figure 3. The delay-shift versus the value of $\phi^{(3)}/(\phi^{(2)})^2$ calculated by the simulation and empirical formula.

When n is set to 1, the value of $\phi^{(3)}/\left(\phi^{(2)}\right)^2$ equals 0.42 ns^{-1}, which was the experimental value in the above CPA system.

As depicted in Figure 3, the delay-shift obtained by the numerical simulation (blue triangle) was almost proportional to the value of $\phi^{(3)}/\left(\phi^{(2)}\right)^2$, which was similar to the empirical formula (red line). When n equaled 1/4, corresponding to the value of $\phi^{(3)}/\left(\phi^{(2)}\right)^2$ being 0.1 ns^{-1}, the delay-shifts were 2.5 and 2.2 ps calculated by the numerical simulation and empirical formula, respectively. The deviation between the numerical simulation and the empirical formula was 0.3 ps. When n increased to 4, corresponding to the value of $\phi^{(3)}/\left(\phi^{(2)}\right)^2$ increasing to 1.7 ns^{-1}, the delay-shift obtained by the numerical simulation increased to 32 ps. Meanwhile, the delay-shift calculated by the empirical formula was 34.5 ps, which was 2.5 ps larger than the simulation result. The possible reasons for the deviation between the simulation and empirical formula are similar to those given in the discussion in Section 3.1, which could be that other high-order dispersion and temporal distortion of pre-pulses were neglected in the empirical formula.

5. Conclusion

In conclusion, we proposed a simple and effective empirical formula to calculate the delay-shift of the pre-pulse, which was independent of the pulse amplifier and the pulse stretcher. This formula was verified in two typical ultra-intense systems. One was a CPA system centered at 800 nm with a single-grating Offner stretcher. The other was an OPCPA system centered at 925 nm with a double-grating Offner stretcher. In both systems, the empirical formula is in good agreement with the experimental results, and the delay-shift was almost proportional to the square of the initial delay of the post-pulse. Numerical simulation was also carried out to further confirm the empirical formula. It was validated that the delay-shift in the numerical simulation was almost proportional to the value of $\phi^{(3)}/\left(\phi^{(2)}\right)^2$, like the empirical

https://doi.org/10.1017/hpl.2024.45 Published online by Cambridge University Press

formula. This work revealed the main factors that influenced the delay-shift value of the pre-pulse, which were the initial delay of the post-pulse and the ratio of TOD to GDD square. Besides, our work could provide useful guidelines for identifying the real source of the pre-pulse and improving the pre-pulse contrast in ultra-intense laser facilities.

Acknowledgements

This work was supported by the National Key Research and Development Program of China (Nos. 2022YFE0204800, 2022YFA1604401 and 2019YFF01014401), the Shanghai Sailing Program (No. 21YF1453800), the National Natural Science Foundation of China (Nos. 11127901 and 61925507), the International Partnership Program of the Chinese Academy of Sciences (No. 181231KYSB20200040), the Shanghai Science and Technology Committee Program (Nos. 22560780100 and 23560750200), the Chinese Academy of Sciences President's International Fellowship Initiative (No. 2023VMB0008) and the Youth Innovation Promotion Association of the Chinese Academy of Sciences.

References

1. W. Li, Z. Gan, L. Yu, C. Wang, Y. Liu, Z. Guo, L. Xu, M. Xu, Y. Hang, Y. Xu, J. Wang, P. Huang, H. Cao, B. Yao, X. Zhang, L. Chen, Y. Tang, S. Li, X. Liu, S. Li, M. He, D. Yin, X. Liang, Y. Leng, R. Li, and Z. Xu, Opt. Lett. **43**, 5681 (2018).
2. C. N. Danson, C. Haefner, J. Bromage, T. Butcher, J.-C. F. Chanteloup, E. A. Chowdhury, A. Galvanauskas, L. A. Gizzi, J. Hein, D. I. Hillier, N. W. Hopps, Y. Kato, E. A. Khazanov, R. Kodama, G. Korn, R. Li, Y. Li, J. Limpert, J. Ma, C. H. Nam, D. Neely, D. Papadopoulos, R. R. Penman, L. Qian, J. J. Rocca, A. A. Shaykin, C. W. Siders, C. Spindloe, S. Szatmári, R. M. G. M. Trines, J. Zhu, P. Zhu, and J. D. Zuegel, High Power Laser Sci. Eng. **7**, e54 (2019).
3. T. J. Yu, S. K. Lee, J. H. Sung, J. W. Yoon, T. M. Jeong, and J. Lee, Opt. Express **20**, 10807 (2012).
4. J. Hu, X. Wang, Y. Xu, L. Yu, F. Wu, Z. Zhang, X. Yang, P. Ji, P. Bai, X. Liang, Y. Leng, and R. Li, Appl. Opt. **60**, 3842 (2021).
5. J. Bromage, S.-W. Bahk, I. A. Begishev, C. Dorrer, M. J. Guardalben, B. N. Hoffman, J. Oliver, R. G. Roides, E. M. Schiesser, M. J. Shoup, M. Spilatro, B. Webb, D. Weiner, and J. D. Zuegel, High Power Laser Sci. Eng. **7**, e4 (2019).
6. X. Wang, X. Liu, X. Lu, J. Chen, Y. Long, W. Li, H. Chen, X. Chen, P. Bai, Y. Li, Y. Peng, Y. Liu, F. Wu, C. Wang, Z. Li, Y. Xu, X. Liang, Y. Leng, and R. Li, Ultrafast Sci. **2022**, 9894358 (2022).
7. F. Lureau, G. Matras, O. Chalus, C. Derycke, T. Morbieu, C. Radier, O. Casagrande, S. Laux, S. Ricaud, G. Rey, A. Pellegrina, C. Richard, L. Boudjemaa, C. Simon-Boisson, A. Baleanu, R. Banici, A. Gradinariu, C. Caldararu, B. D. Boisdeffre, P. Ghenuche, A. Naziru, G. Kolliopoulos, L. Neagu, R. Dabu, I. Dancus, and D. Ursescu, High Power Laser Sci. Eng. **8**, e43 (2020).
8. H. Kiriyama, A. S. Pirozhkov, M. Nishiuchi, Y. Fukuda, K. Ogura, A. Sagisaka, Y. Miyasaka, M. Mori, H. Sakaki, N. P. Dover, K. Kondo, J. K. Koga, T. Z. Esirkepov, M. Kando, and K. Kondo, Opt. Lett. **43**, 2595 (2018).
9. C. Bernert, S. Assenbaum, S. Bock, F.-E. Brack, T. E. Cowan, C. B. Curry, M. Garten, L. Gaus, M. Gauthier, R. Gebhardt, S. Göde, S. H. Glenzer, U. Helbig, T. Kluge, S. Kraft, F. Kroll, L. Obst-Huebl, T. Püschel, M. Rehwald, H.-P. Schlenvoigt, C. Schoenwaelder, U. Schramm, F. Treffert, M. Vescovi, T. Ziegler, and K. Zeil, Phys. Rev. Appl. **19**, 014070 (2023).
10. M. Kaluza, J. Schreiber, M. I. K. Santala, G. D. Tsakiris, K. Eidmann, J. Meyer-ter Vehn, and K. J. Witte, Phys. Rev. Lett. **93**, 045003 (2004).
11. L. Yu, Y. Xu, Y. Liu, Y. Li, S. Li, Z. Liu, W. Li, F. Wu, X. Yang, Y. Yang, C. Wang, X. Lu, Y. Leng, R. Li, and Z. Xu, Opt. Express **26**, 2625 (2018).
12. D. N. Papadopoulos, P. Ramirez, K. Genevrier, L. Ranc, N. Lebas, A. Pellegrina, C. L. Blanc, P. Monot, L. Martin, J. P. Zou, F. Mathieu, P. Audebert, P. Georges, and F. Druon, Opt. Lett. **42**, 3530 (2017).
13. Y. Li, B. Shao, Y. Peng, J. Qian, W. Li, X. Wang, X. Liu, X. Lu, Y. Xu, Y. Leng, and R. Li, High Power Laser Sci. Eng. **11**, e5 (2023).
14. M. P. Kalashnikov, E. Risse, H. Schönnagel, and W. Sandner, Opt. Lett. **30**, 923 (2005).
15. L. Yu, Y. Xu, S. Li, Y. Liu, J. Hu, F. Wu, X. Yang, Z. Zhang, Y. Wu, P. Bai, X. Wang, X. Lu, Y. Leng, R. Li, and Z. Xu, Opt. Express **27**, 8683 (2019).
16. H. Chen, X. Wang, X. Liu, Y. Long, W. Li, X. Chen, P. Bai, J. Hu, F. Wu, Z. Zhang, Y. Liu, Y. Xu, and Y. Leng, Appl. Phys. B. **129**, 55 (2023).
17. F. Tavella, A. Marcinkevičius, and F. Krausz, New J. Phys. **8**, 219 (2006).
18. S. Roeder, Y. Zobus, C. Brabetz, and V. Bagnoud, High Power Laser Sci. Eng. **10**, e34 (2022).
19. C. Dorrer and J. Bromage, Opt. Express **16**, 3058 (2008).
20. N. Khodakovskiy, M. Kalashnikov, E. Gontier, F. Falcoz, and P.-M. Paul, Opt. Lett. **41**, 4441 (2016).
21. B. Webb, C. Feng, C. Dorrer, C. Jeon, R. G. Roides, S. Bucht, and J. Bromage, Opt. Express **32**, 12276 (2024).
22. X. Lu, H. Zhang, J. Li, and Y. Leng, Opt. Lett. **46**, 5320 (2021).
23. C. Hooker, Y. Tang, O. Chekhlov, J. Collier, E. Divall, K. Ertel, S. Hawkes, B. Parry, and P. P. Rajeev, Opt. Express **19**, 2193 (2011).
24. L. Ranc, C. L. Blanc, N. Lebas, L. Martin, J.-P. Zou, F. Mathieu, C. Radier, S. Ricaud, F. Druon, and D. Papadopoulos, Opt. Lett. **45**, 4599 (2020).
25. P. Bai, Z. Zhang, X. Wang, F. Wu, J. Hu, X. Yang, J. Qian, J. Gui, X. Lu, Y. Liu, Y. Xu, X. Liang, Y. Leng, and R. Li, Appl. Opt. **61**, 4627 (2022).
26. X. Wang, P. Bai, Y. Liu, H. Zhang, Y. Tang, X. Wang, X. Zhang, C. Fan, B. Yao, Y. Sun, F. Wu, Z. Zhang, Z. Gan, L. Yu, C. Wang, X. Lu, Y. Xu, X. Liang, and Y. Leng, Opt. Lett. **47**, 5164 (2022).
27. D. N. Schimpf, E. Seise, J. Limpert, and A. Tünnermann, Opt. Express **16**, 10664 (2008).
28. N. Didenko, A. Konyashchenko, A. Lutsenko, and S. Tenyakov, Opt. Express **16**, 3178 (2008).
29. J. Wang, P. Yuan, J. Ma, Y. Wang, G. Xie, and L. Qian, Opt. Express **21**, 15580 (2013).
30. X. Wang, X. Lu, X. Guo, R. Xu, and Y. Leng, Opt. Lett. **16**, 053201 (2018).
31. H. Kiriyama, Y. Miyasaka, A. Kon, M. Nishiuchi, A. Sagisaka, H. Sasao, A. S. Pirozhkov, Y. Fukuda, K. Ogura, K. Kondo, N. P. Dover, and M. Kando, High Power Laser Sci. Eng. **9**, e62 (2021).
32. X. Chen, X. Wang, H. Chen, X. Yang, J. Hu, P. Bai, Y. Zhao, S. Pan, F. Wu, Z. Zhang, Y. Xu, and Y. Leng, Appl. Opt. **62**, 7791 (2023).

https://doi.org/10.1017/hpl.2024.45 Published online by Cambridge University Press

33. H. Chen, X. Wang, X. Liu, X. Chen, P. Bai, S. Pan, L. Hu, J. Hu, F. Wu, Z. Zhang, Y. Liu, Y. Xu, and Y. Leng, Opt. Express **31**, 40285 (2023).
34. Y. Xu, J. Lu, W. Li, F. Wu, Y. Li, C. Wang, Z. Li, X. Lu, Y. Liu, Y. Leng, R. Li, and Z. Xu, Opt. Laser Technol. **79**, 141 (2016).
35. F. Wu, Z. Zhang, X. Yang, J. Hu, P. Ji, J. Gui, C. Wang, J. Chen, Y. Peng, X. Liu, Y. Liu, X. Lu, Y. Xu, Y. Leng, R. Li, and Z. Xu, Opt. Laser Technol. **131**, 106453 (2020).
36. F. Wu, X. Liu, X. Wang, J. Hu, X. Lu, Y. Li, Y. Peng, Y. Liu, J. Chen, Y. Long, W. Li, Z. Zhang, Y. Xu, C. Wang, Y. Leng, and R. Li, Opt. Laser Technol. **148**, 107791 (2022).

https://doi.org/10.1017/hpl.2024.45 Published online by Cambridge University Press